

Development of a Bendable Permanent-Magnet Tubular Linear Motor

Christian Urban, Richard Günther, Thomas Nagel, René Richter, and Robert Witt

Faculty of Electrical Engineering and Information Technology, Institute of Electromechanical and Electronic Design, Dresden University of Technology, Dresden 01062, Germany

This paper presents a new flexible linear actuator. It is a two-phase permanent-magnet tubular linear motor. An elastomer offers the desired actuator flexibility both between the coils of the stator and between the magnets in the mover. We determined the motor dimensions in a numerical parameter optimization and used various finite element models. The novel artificial muscle actuator is designed for tensile loads. It is electrically powered and obtains variable forces. Weights up to 750 g were lifted with a minimal bending radius of 200 mm. The outer diameter of the flexible linear direct drive measures about 30 mm.

Index Terms—Bendable linear actuator, electric propulsion, flexible linear actuator, tubular linear permanent-magnet motors.

I. INTRODUCTION

ELECTROMAGNETIC linear direct drives are able to realize high forces, large strokes, high reliability, and fast response [1], [2]. A bendable actuator combining these advantages might extend the moving range and the flexibility in robotics.

For example, there are ambitions to build a power assist suit with flexible electric powered actuators [3]. Although there are bendable pneumatic muscle actuators (PMA) [4], a bendable electromagnetic linear motor neither needs bulky valves and piping nor compressors.

The flexible linear electromagnetic actuator described in [3] is a bendable asynchronous tubular linear motor with a thrust force of 50 mN.

Not only the efficiency of a permanent-magnet tubular linear motor (PMTLM) seems to be better, but also the achievable thrust forces are significantly higher [5], [6], and [7].

A PMTLM with a slotted stator iron and a nonferromagnetic material between the permanent magnets (PM) in the mover is described in [8]. This variant has lower transverse forces. A slotted PMTLM with a separate iron core for each coil is described in [9]. Its stator is built up modular to simplify the variation of the stator design.

In contrast to these PMTLMs, we inserted flexible elements between the coils of the stator and replaced the ferromagnetic rings in the mover by elastomer rings. These two modifications make the motor bendable. The new developed flexible actuator allows less rigid robot constructions.

In this paper we present the main aspects of the development starting with the structure of the new bendable linear motor, continuing with the analysis of the actuators flexibility and magnetic field calculations. Finally, we characterize the flexible linear actuator in the experimental investigations.

Manuscript received August 24, 2011; revised October 11, 2011 and February 16, 2012; accepted March 06, 2012. Date of publication March 12, 2012; date of current version July 20, 2012. Corresponding author: R. Günther (e-mail: richard.guenther@ifte.de).

Color versions of one or more of the figures in this paper are available online at <http://ieeexplore.ieee.org>.

Digital Object Identifier 10.1109/TMAG.2012.2190613

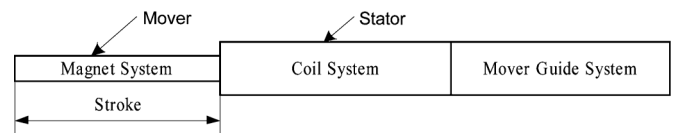


Fig. 1. Basic structure of the bendable linear actuator.

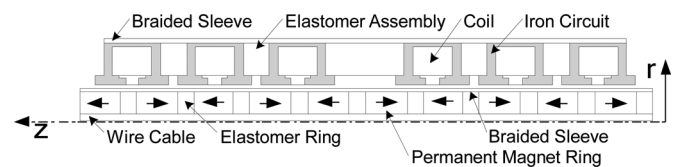


Fig. 2. Schematic construction of the active motor part (section: coil system).

II. STRUCTURE

Although motors with three or more phases have lower vibration and better performance [10], we chose a two-phase stepper motor, because it is easier to control. Beside this, the main focus of this study was to realize the bendability. Our motor is intended as an actuator for tensile loads. The basic structure is shown in Fig. 1.

The stator consists of a coil system and a mover guide system, which allows a length variation of the whole actuator. The magnet system in the mover is equipped with permanent magnets with an alternate polarity. The length variation ratio of the bendable actuator is about 50%, so, the mover is twice as long as the coil system. The schematic construction of the stator and the mover in the section of the coil system is shown in Fig. 2. It is a tubular linear motor. The axis of rotation is the Z -axis.

The stator contains the coils with its iron circuit for magnetic flux guide and the guide for the mover. The flexibility of the stator is realized by elastomer assemblies between them. The stator is covered with a braided sleeve made of tinned copper. This prevents axial length changes of the stator which could occur due to tensile elongations of the elastomer assemblies. However, it does not impede bending of the stator. Furthermore, the cooling surface of the motor increases due to its good heat conductivity. Therefore, the heat of the coil system is dissipated to the environment even in the section of the mover guide system.

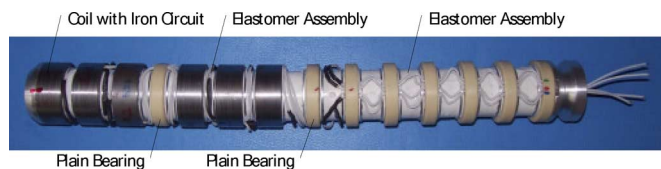


Fig. 3. Stator of the bendable linear actuator without the sleeve.

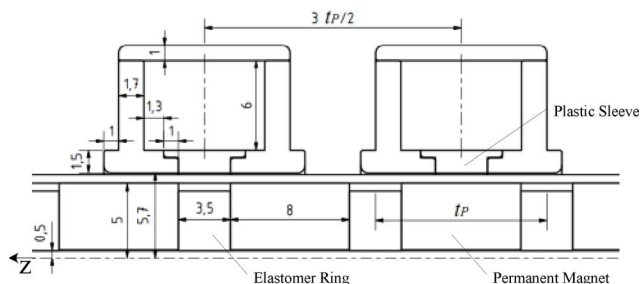


Fig. 4. Motor dimensions.

To avoid electric short circuits, we inserted an insulating tape between the self supporting coils and the iron core.

The axially magnetized ring magnets in the mover are strung on a steel wire. Elastomer rings between them enable the bend of the mover. A PET braided sleeve covers the mover. In the section of the coil system of the stator this sleeve directly slides inside the iron circuits of the coils. So the air gap of the motor is minimized.

Fig. 3 shows the stator of the flexible linear motor without the braided sleeve.

An extra plain bearing centers the mover in the stator coil system. The elastomer assemblies in the mover guide system are wider than those between the coils. In this way, the end of the stator is more flexible than the section with the coil system. The final dimensions of the iron circuit and the magnets are shown in Fig. 4.

The dimensions of the motor were found in a numerical parameter optimization. The pole pitch t_P complies with the length of a permanent magnet and an elastomer ring. The iron circuit is made of 9SMn28k (1.0715). We inserted a plastic sleeve between the two turned iron parts with a special friction behavior. The slot inside the iron circuit enables the centering and fixing of these plastic sleeves. The iron pipe provides the mechanical strength. If a permanent magnet is situated between the iron circuits of two coils, the field intensity in the iron parts at the side will be higher than in the outer back iron. This is caused by the fact that the field lines of two magnets pass these parts at the side simultaneously. Therefore, these iron parts are wider. The pole shoes are chamfered on the outside of the iron circuit. As a result the braided sleeve of the mover cannot cant. The outer diameter of the elastomer rings in the mover is smaller than the diameter of the magnets. If the elastomer is compressed by axial forces it will be bulged outwards. The manufactured prototype of the bendable linear motor is shown in Fig. 5.

The stator has a length of 253 mm and the outer diameter measures about 30 mm. The diameter of the mover measures



Fig. 5. Bendable linear motor.

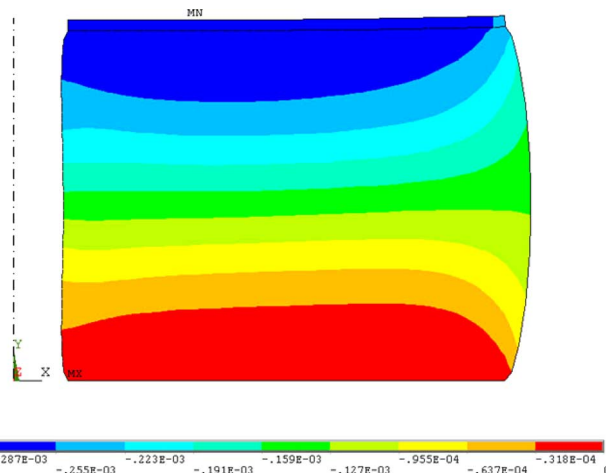


Fig. 6. Axial displacement (m) of the elastomer ring in the mover for a pressure load (2-D axisymmetric FE model, axis of rotation is Y).

about 11 mm. The maximum stroke of the bendable linear motor is 115 mm.

III. ACTUATOR FLEXIBILITY

The axial length variation between the coils in the stator and between the magnets in the mover should be as low as possible. The necessary bending force should be very low as well. In different structural simulations with ANSYS, we analyzed the axial displacement and the bend of the elastomer ring in the mover.

A. Mover Elastomer Ring

In a two-dimensional axisymmetric FE model, the axial displacement caused by a load of 30 N on the top of the elastomer was simulated. The elastomer ring in the mover consists of a silicone with a shore-A-hardness of 50. The axial displacement is shown in Fig. 6.

For this load case the axial displacement of the elastomer ring is about 0.3 mm. The maximal mechanical strain is about 43%.

The breaking strain for the selected silicone is about 100%. The bend of the elastomer ring was analyzed in a three-dimensional FE model of a section of the mover. Different symmetry relationships were used. The model is symmetrically to the YZ-Plane and to the XY-Plane. As a result, the model contains

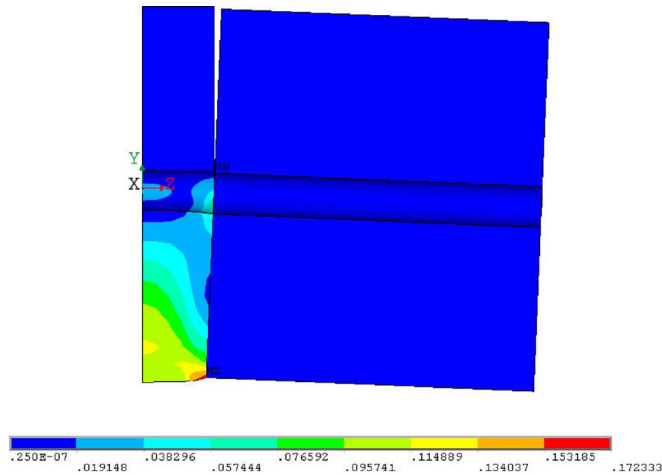


Fig. 7. Mechanical strain of the elastomer caused by the bend of the mover.

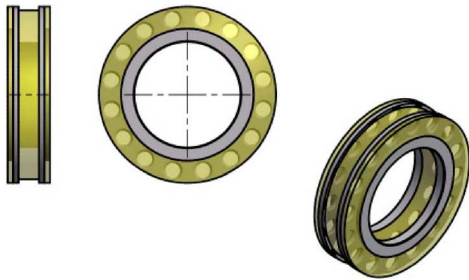


Fig. 8. Elastomer assembly of the stator in the section of the coil system.

only a quarter of the elastomer ring and a half of the magnet as shown in Fig. 7.

For a bending radius of 123 mm the mechanical strain is about 17%. This is below the breaking strain, too.

B. Stator Elastomer Assembly

A form closure between the silicone and two aluminum rings in this assembly was designed. It was possible to realize a centering and fixation of the stator elastomer assembly. Furthermore, an axial compression effects a lower displacement than an axial elongation. While bending, the material in the holes is more loaded than the rest of the silicone. The stator elastomer assembly for the section of the coil system is shown in Fig. 8.

The elastomer assemblies of the stator in the section of the mover guide system are just wider. The elastomer assemblies for the stator and the silicone rings for the mover were manufactured in using casting molds made of aluminum. A silicone with a shore-A-hardness of 30 and a breaking strain of 200% was used for the stator elastomer assemblies. It withstands a bending radius of 200 mm. The used silicone in the mover would not resist those high tensions.

IV. MAGNETIC FIELD CALCULATIONS

A. Unbent Motor

The axial force of the unbent motor was calculated with the two-dimensional axisymmetric FE model of the motor. This simulation system was used for the parameter optimization. The

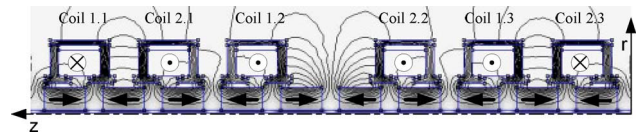


Fig. 9. Field distribution for excitation of all coils.

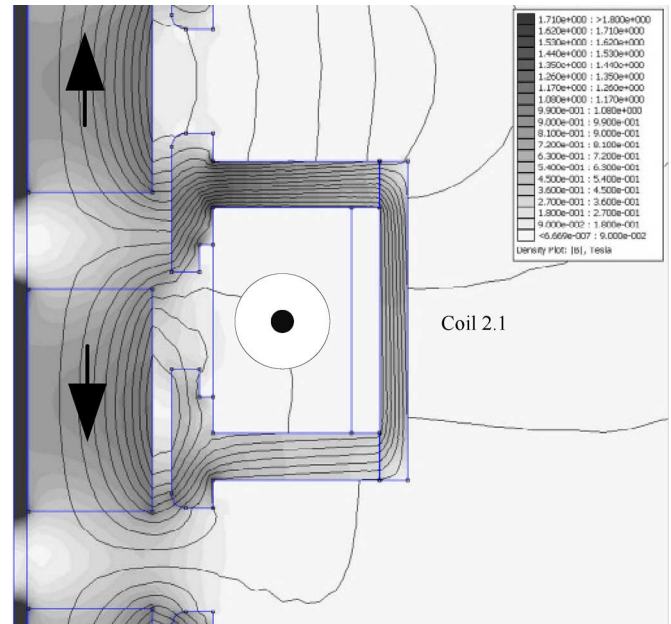


Fig. 10. Detail of the field distribution for excitation of all coils.

field distribution of the bendable motor for excitation of all coils is shown in Fig. 9.

In [11] and [12] an optimization was successfully used to improve the geometry of electromagnetic linear motors. Optimization criteria were the maximization of the force density and the minimization of the thrust ripple. The optimization objective was to achieve a sinusoidal force characteristic with large amplitude. Design parameters were the dimensions of the magnets and the pole shoes of the iron circuit. Additionally, the diameter of the winding wire and the distance between the magnets in the mover were varied. We used the program FEMM 4.2 for simulation and found the dimensions of the motor in a numerical parameter optimization with the program OptiY 4.0. The used NdFeB neodym permanent magnets have a grade of 50 M, a coercive force H_C of 1033 kA/m, and a remanence B_R of 1.4 T. The magnetization was simplified by a temperature independent material linearity ($\mu_r = 1.05$) for room temperature.

The wire cable in the mover is made of steel. Inside the magnets, the steel is in saturation as shown in Fig. 10. However, the influence to the characteristic force curve is negligible. Nevertheless, a nonmagnetic material for the wire cable should be preferred.

The characteristic force curve is calculated for a length of two magnets and two elastomer rings, which is twice the pole pitch.

We studied different arrangements of the coils and varied the number of coils as well as the distance between them. The best results for the characteristic force curve were reached by the arrangement shown in Fig. 9. The phase 1 contains the coils

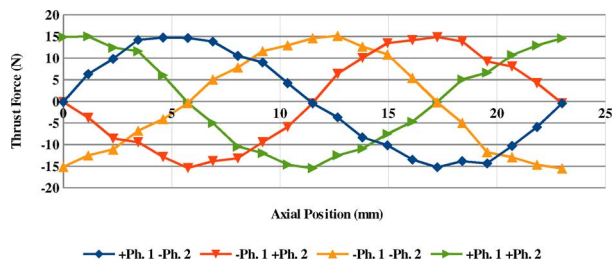


Fig. 11. Simulated motor force characteristic curves (9.1 W motor power).

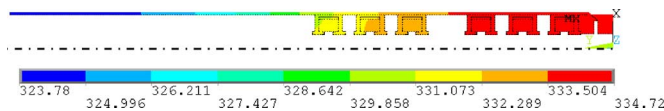


Fig. 12. Axisymmetric thermal 2-D FE-model with temperature distribution in Kelvin of the powered motor (9.1 W motor power).

1.1, 1.2, and 1.3 and the phase 2 the coils 2.1, 2.2, and 2.3. The larger gap between the coils in the center of the coil system improves the symmetry of the motor. As a result, two magnets and two elastomer rings between the iron circuits of two coils are always arranged side by side. The characteristic force curves of the motor for the various phase energizations are shown in Fig. 11.

The calculated force amplitude for a continuous duty is about 15 N. The design of the iron circuit has an enormous influence on the characteristic force curve. We limited the electric power for a continuous duty of the motor to 9.1 W. The diameter of the winding wire is 0.3 mm. The number of turns for each coil is 320. Therefore, the continuous current for each phase of the coil system is 0.53 A. In this case, the current density is 7.4 A/mm².

All iron circuits are equal, but the winding direction of the coils is different as shown in Fig. 9 as well.

The electric power of 9.1 W was determined analytically with a thermal FE-model for a surface temperature of 50°C at the coilless end of the motor. This model contains the coils including the iron core and the braided copper sleeve (cf. Fig. 12). Temperature inside the motor is assumed to be as high as in the iron core as the stationary mover can hardly emit heat. The motor gives off heat by convection and radiation. Convection is expressed by a heat transfer coefficient. It respects the motor shape and the kind of convection. In continuous operation with an electrical power of 9.1 W the magnets heat up to 60°C. However, a magnetic flux density of about 0.3 T inside the magnets can cause demagnetization for this arrangement at temperatures above 40°C. There are several possibilities to avoid this problem. A temperature of 40°C could be reached by a motor power of 4 W or by a forced convection with 5 m/s air speed. However, both possibilities are unacceptable. The use of pole shoes with a thickness of 2 mm at the front of the magnets is an alternative. These would guide the field lines radially out of the mover in a better way and prevent demagnetization. Disadvantages of this variant are higher production costs, a lower positioning accuracy, and a lower power density. The best option seems to be the usage of magnets with a grade of 48 H. They have a specified maximum operating temperature of 120°C and demagnetization should not occur for a temperature of up to

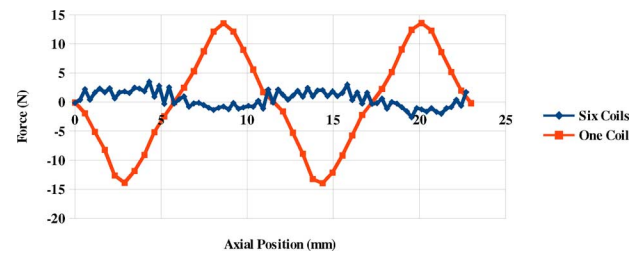


Fig. 13. Simulated motor force characteristics curve (unpowered).

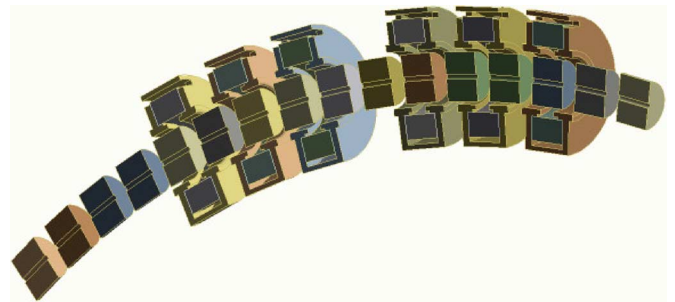


Fig. 14. CAD model of motor for electromagnetic simulation (bending radius 200 mm).

80°C for the used arrangement. The motor force would be reduced by about 5%.

B. Unpowered Unbent Motor

The dimensions of the iron circuit were optimized in order to reach a sinusoidal characteristic force curve for the powered actuator. In addition, we calculated the characteristic force curves for all coils of the unpowered bendable linear actuator and for a single coil. The force onto the mover versus the axial position is shown in Fig. 13.

The calculated maximum holding force for one unpowered coil is 13.6 N. We identified a value of 15.4 N in a force measurement. The influence of the friction was not considered in this simulation. In the FE analysis with all coils unpowered the maximum holding force was only 3.5 N.

C. Bent Motor

A three-dimensional FEM simulation was implemented to characterize the bent linear motor. First of all, a structural 3-D simulation was performed to determine the angle between two adjacent magnets or coils depending on the bending radius. Based on this the model for electromagnetic simulation was built. Bending radius, mover position, and energization were varied to get the desired simulation results. The belt friction between the bent components was considered using the capstan equation with an experimentally determined friction coefficient of 0.25. Displacements of coils and magnets due to the magnetic forces and other friction losses have been neglected. As shown in Fig. 14 one symmetry plane was used.

For smaller bending radii the force amplitude increases whereas the overall quality of the motor characteristic decreases (cf. Fig. 15). This is due to the fast growing coil spacing in comparison to the magnet spacing.

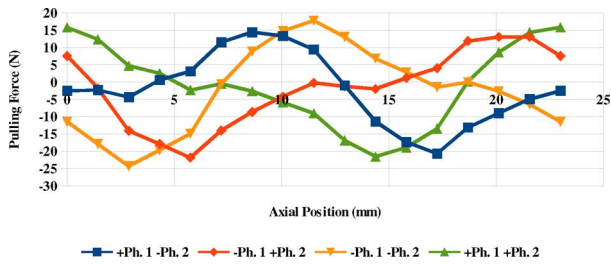


Fig. 15. Simulated motor force characteristic curves (9.1 W motor power and 200 mm bending radius).

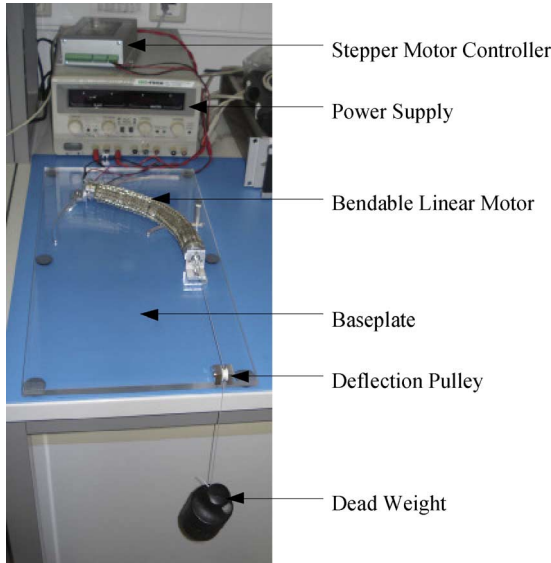


Fig. 16. Test bench of the bendable linear motor.

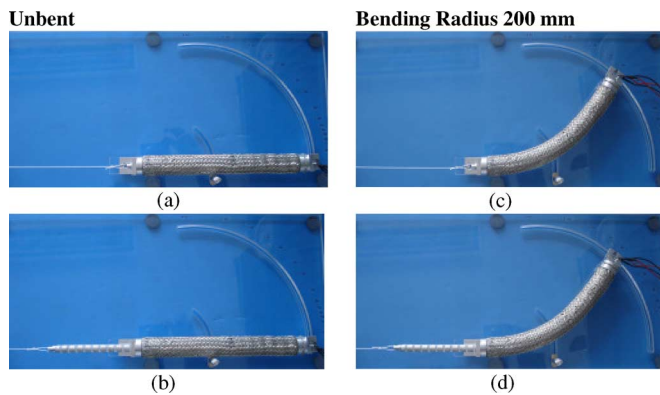


Fig. 17. Bend of the linear motor: (a) minimal stroke, (b) maximal stroke, (c) minimal stroke, (d) maximal stroke.

V. EXPERIMENTAL INVESTIGATIONS

A. Test Bench

The proof of function of the motor was rendered in the related test bench shown in Fig. 16.

The flexible linear motor is fixed on a baseplate. The minimal adjustable bending radius is 100 mm. Weights can be lifted by the use of a deflection pulley. The bend of the motor is shown in Fig. 17.

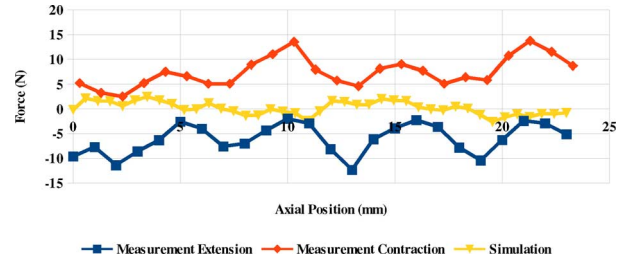


Fig. 18. Measured motor force characteristic curves compared to simulation (unpowered).

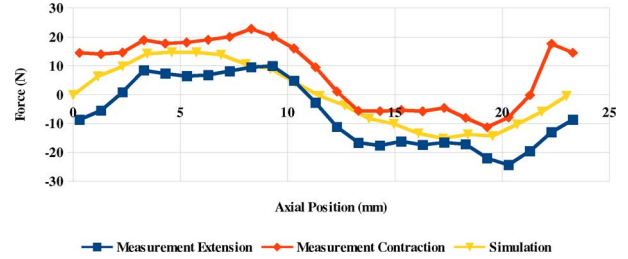


Fig. 19. Measured motor force characteristic curves for energization variant Phase 1 positive and Phase 2 negative compared to simulation.

The minimal bending radius of the motor is limited by the breaking elongation of the elastomer assemblies of the stator. The flexible linear motor was designed for a minimal bending radius of 200 mm. Smaller bending radii should be possible with a different elastomer or design of the elastomer assembly. After 20 full steps of the motor, the maximal stroke of 115 mm is achieved. The maximal step frequency is 150 Hz. This corresponds to a velocity of about 0.9 m/s. To reach higher velocities, the frequency should be increased during the startup period.

B. Force Characteristic

The characteristic force curves were measured with the unbent motor. A force gauge was rigidly coupled with the mover and displaced with a linear guiding.

The characteristic for the unpowered motor is shown in Fig. 18. A more or less constant offset is clearly visible between the extension and the contraction force. It primarily results from the friction of the motor. The ripple of the unpowered motor is nearly 11 N, which is greater than the simulated ripple of 6 N. This is mainly caused by the axial displacement of the coils and magnets due to the used elastomer assemblies.

For the measurements with powered coils, the current in every phase was 0.55 A. The resulting power was 9.2 W. An offset caused by the friction is also detectable for these characteristics (Fig. 19). The identified friction is nearly 7 N and approximately complies with the friction of the unpowered motor.

Figs. 20 and 21 show the individual energization variants for the contracting motor compared to the simulation. The measured curves have a positive offset due to the friction. Furthermore, they deviate from the sinusoidal shape. This results from the displacement of the coils and magnets due to the elastomer assemblies. The measured motor force characteristics for all energization variants of the contracting motor are presented in Fig. 22. It can be seen that the difference between maximum

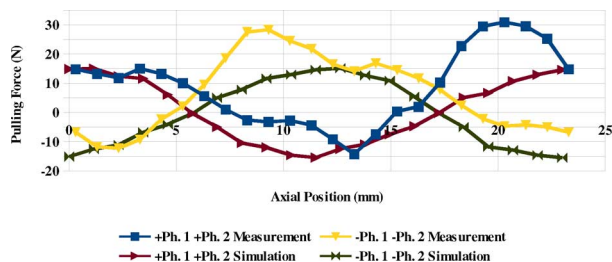


Fig. 20. Measured motor force characteristic curves for energization variant +Ph. 1 +Ph. 2 and -Ph. 1 -Ph. 2 compared to simulation for motor contraction.

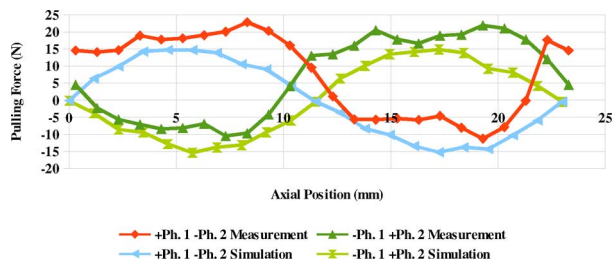


Fig. 21. Measured motor force characteristic curves for energization variant +Ph. 1 -Ph. 2 and -Ph. 1 +Ph. 2 compared to simulation for motor contraction.

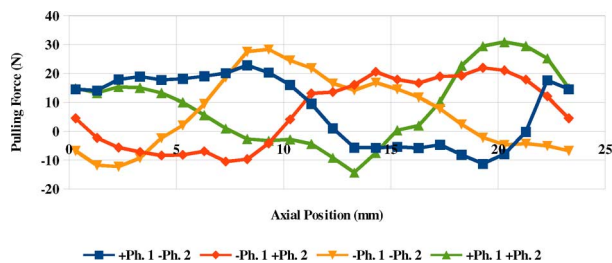


Fig. 22. Measured motor force characteristic curves for motor contraction.

and minimum force for an energization variant ranges from 32 to 41 N. These values are greater than the simulated 30 N. The maximum holding force is up to 31 N and the pulling force about 3 N compared to 15 N and 9 N in the simulation without friction. These differences also result from the axial displacement of the coils and magnets.

C. Restoring Force

We measured the restoring forces at the end of the motor depending on the bending radius with and without the retracted mover. The results are shown in Fig. 23. It is not possible to show constant spring stiffness. For smaller radii the motor stiffens increasingly. The viscoelasticity of the elastomer is not considered in this measurement. It would cause a reduction of the restoring force for deformations over a longer period of time.

D. Pulling Forces

Different weights have been lifted and the bending radius has been varied to identify the performance of the motor. The required current versus the bending radius compared to 3-D simulations is shown in Fig. 24.

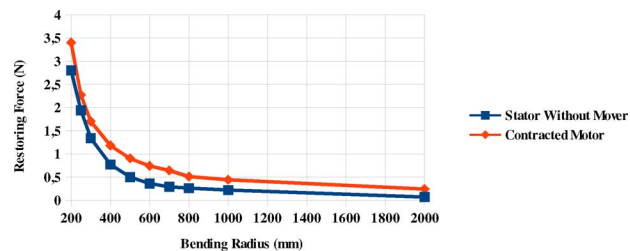


Fig. 23. Measured restoring force versus the bending radius.

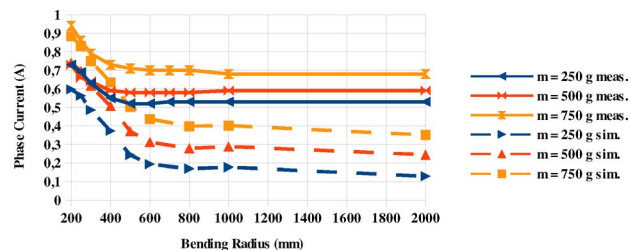


Fig. 24. Measurements and simulation of motor current versus the bending radius of the actuator for three different loads.

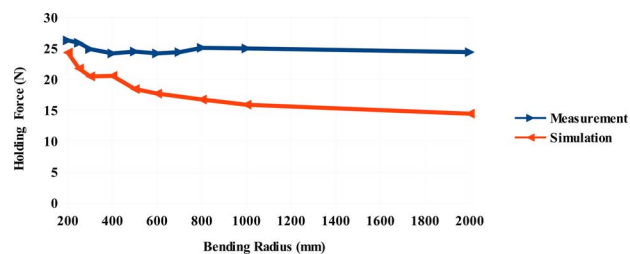


Fig. 25. Measured and simulated holding force of the motor versus the bending radius for energization variant +Ph. 1 -Ph. 2 (9.1 W motor power).

Down to a bending radius of 400 mm the motor current is nearly constant. In contrast the simulation shows a slight decrease of the motor current for a rising bending radius. The reason is an axial displacement of the coils by magnetic forces for a weak bending of the real motor. This has a negative effect on the pulling force. The general higher currents for large bending radii are also caused by the significant amplification of the friction forces due to the radial displacement of the mover. In measurements as well as in simulation considerably more current is needed for smaller bending radii. The fast growing coil spacing in comparison to the magnet spacing is the main reason for that increase.

E. Maximum Holding Force

The maximum holding force of the motor for the continuous current is shown in Fig. 25.

We measured the maximum holding force for a constant current of 0.53 A. The force is in the range between 24 N and 26 N. For small bending radii an increase of the holding force is recognizable, caused by the higher force amplitudes (cf. Section IV-C). The simulation indicates small holding forces for large bending radii. For a more extensive bending the simulation approaches to the measurement. The main reason for the deviation should be the axial displacement of the coils and magnets, again.

VI. CONCLUSION

The integration of elastomer assemblies to a tubular permanent-magnet linear motor enabled the construction of a bendable linear actuator. An electric powered bendable actuator for tensile loads was developed. For this purpose the geometry was optimized to get a sinusoidal force characteristic.

The motor has a length of 253 mm and a maximum stroke of 115 mm. A remarkable minimum bending radius of 200 mm is reached. Furthermore a holding force density of 49 N/kg in continuous operation is achievable. The thrust force density of 6 N/kg is significantly lower. Similar motors of larger size, e.g., for application in industrial robots, could be realized as well. On the one hand, the current density has to be reduced when increasing the coil dimensions. While the current density of the presented motor is 7.4 A/mm² for larger motors a current density of 2–4 A/mm² is recommended [13]. On the other hand the partial influence of air gaps and production tolerances can be reduced, thus increasing the force density.

The friction in unbent state is nearly 7 N. It results from the surface of the PET braided sleeve and the loose fit between stator and mover. This loose fit is necessary for providing the bendability but causes an increased radial force.

The measured force characteristic differs from the desired sinusoidal shape. A modified design reducing or preventing the axial relative displacements of the coils and magnets would improve the characteristic. Although this could be reached by using stiffer elastomer components, it would also increase the bending stiffness resulting in higher restoring forces and friction. This contradiction is subject of further optimization.

Bending the motor reduces the pulling force. This is caused by rising friction due to restoring forces, but mainly by increase of distances between the coils. The motor should be modified to get as nearly as possible the same growing of coil spacing and magnet spacing while bending. One possibility is to minimize the outer diameter of the stator elastomer assemblies.

Although the described effects cause differences between the simulated and measured thrust and holding forces they have the same order of magnitude. Especially considering the friction of the real motor there is a good correlation between simulated and measured results.

Furthermore the permanent magnets should be replaced by magnets with a higher maximum operating temperature to prevent demagnetization.

Another field of interest is the self-locking for this flexible linear actuator. Thus, the power consumption for holding a defined motor position could be reduced.

ACKNOWLEDGMENT

The authors wish to thank D. Pahner and C. Ullmann for their contributions in this field of activities.

REFERENCES

- [1] R. C. Okonkwo and R. Hanitsch, "Development and control of a prototype permanent-magnet DC linear motor," *IET Electr. Power Appl.*, vol. 1, no. 2, pp. 223–228, 2007.
- [2] A. W.-J. Hsue, M.-T. Yan, and S.-H. Ke, "Comparison on linear synchronous motors and conventional rotary motors driven wire-EDM processes," *J. Mat. Process. Technol.*, vol. 192–193, pp. 478–485, 2007.
- [3] K. Ohyama, Y. Hyakutake, and H. Kino, "Verification of operating principle of flexible linear actuator," in *IEEE Int. Conf. ICEMS*, 2009, pp. 1–6.
- [4] M. B. Pritts and C. D. Rahn, "Design of an artificial muscle continuum robot," in *IEEE Int. Conf. ICRA*, 2004, pp. 4742–4746.
- [5] N. Bianchi, S. Bolognani, D. D. Corte, and F. Tonel, "Tubular linear permanent magnet motors: An overall comparison," *IEEE, Trans. Ind. Appl.*, vol. 39, no. 2, pp. 466–475, Mar./Apr. 2003.
- [6] I.-C. Vese, F. Marignetti, and M. M. Radulescu, "Multiphysics approach to numerical modeling of a permanent-magnet tubular linear motor," *IEEE, Trans. Ind. Electron.*, vol. 57, no. 1, pp. 320–326, Jan. 2010.
- [7] B. Gundelsweiler, "Dimensionierung und Konstruktion von feinerwerk-technischen elektrodynamischen Lineardirektantrieben," Dissertation, University Stuttgart, Stuttgart, Germany, 2003, ISBN-13: 978-3922381228.
- [8] D. Ausderau, "Polysolenoid-Linearantrieb mit genutetem Stator," Diss. ETH Nr. 15498, 2004.
- [9] J. F. Gieras, Z. J. Piech, and B. Tomczuk, *Linear Synchronous Motors: Transportation and Automation Systems*, 2nd ed. Boca Raton, FL: CRC Press, 2011, p. 170.
- [10] B. Tomczuk, G. Schröder, and A. Waindok, "Finite-element analysis of the magnetic field and electromechanical parameters calculation for a slotted permanent-magnet tubular linear motor," *IEEE, Trans. Magn.*, vol. 43, no. 7, pp. 3229–3236, Jul. 2007.
- [11] N. R. Tavana and A. Shoulaie, "Pole-shape optimization of permanent-magnet linear synchronous motor for reduction of thrust ripple," *Energy Convers. Manage.*, vol. 52, pp. 349–354, 2011.
- [12] J. Wang, D. Howe, and W. Jewell, "Analysis and design optimization of an improved axially magnetized tubular permanent-magnet machine," *IEEE, Trans. Energy Conversion*, vol. 19, no. 2, pp. 289–295, Jun. 2004.
- [13] E. Kallenbach, R. Eick, P. Quendt, T. Ströhla, K. Feindt, and M. Kallenbach, *Elektromagnete: Grundlagen, Berechnung, Entwurf und Anwendung*, 3rd ed.: Gable Wissenschaftsverlage, 2008, p. 284.

Christian Urban received the diploma degree in electrical engineering from the University of Technology in Dresden, Germany, in 2010.

He is a Research Assistant at the Institute of Electromechanical and Electronic Design at the Dresden University of Technology.

Richard Günther received the diploma degree in electrical engineering from the University of Technology in Dresden, Germany, in 2009.

Since 2009, he has been a Research Associate at the University of Technology in Dresden. His main research interests are in the field of predevelopment of innovative actuators and medical devices.

Thomas Nagel received the diploma degree in electrical engineering from the University of Technology in Dresden, Germany, in 1986 after his occupational activity as a precision mechanics. In 1990 he received the Ph.D. degree.

In 2005 he was appointed to Assistant Professor of precision mechanics at the University of Technology in Dresden.

René Richter received the diploma degree in electrical engineering from the Dresden University of Technology, Germany, in 2001. He joined the STRI at the University of Hertfordshire, U.K., with a research program focused on micro pumps. In the year 2002 he continued his research in Dresden on micro pumps for drug delivery devices and received his Ph.D. in 2008. Now his main research interests are in the field of medical devices and bio-inspired actuators.

Robert Witt received the diploma degree in electrical engineering from the Dresden University of Technology, Germany, in 2001. Afterwards, he joined the research group for toothed belt drives at the Institute of Electromechanical and Electronic Design in Dresden where he received the Ph.D. degree in 2007 for modelling and simulating the behavior of steel ropes. Now his main research interests are in the field of predevelopment of medical devices, miniature fluidics and biomimetics.